

Parametric Study of Laser Energy Deposition in Mach 8 Bow Shock

Xiaojing Yu and Hong Yan

School of Power and Energy, Northwestern Polytechnical University
127 Youyi Xilu, Xi'an, Shaanxi, China 710072
Corresponding author: yanhong@nwpu.edu.cn

[Received date 3/30/2012; Accepted date 10/22/2012]

ABSTRACT

A numerical study was performed to investigate the effect of laser energy deposition in a Mach 8 bow shock. The computational model was extracted from the experiment in which a nominal two-dimensional Mach 8 flow over a cylinder with diameter of 76 mm was studied. The surface pressure was in good agreement with experiments, and the standoff distance agreed well with the theoretical value. The process of blast wave propagation and bow shock distortion was analyzed for energy deposition. The effect of energy level, deposition location and pulsing frequency was studied. For a single pulse of energy deposition, results showed that the reduction of the time-averaged surface pressure increases beyond certain energy level, while the deposition location had less effect on the time-averaged pressure. For a continuously pulsed deposition, the surface pressure in the stagnation region was reduced with increase of frequency. A 33% pressure reduction was achieved with a frequency of 100 kHz. The envelop of the blast wave formed a conically shaped shock wave in front of the blunt body, resulting in the reduction of the wave drag.

1. INTRODUCTION

Bow shocks in front of blunt body are the main source of drag in hypersonic flying vehicles [1, 2]. How to reduce this wave drag has attracted great attention in recent years. Bushnell [3] had reviewed extant wave drag reduction methods, among which energy deposition off the body had great superiority because of its feasibility and high efficiency. The concept was first put forward in 1950's [4], and experienced a surge in the last decades. Some modern achievements were reviewed by Tretyakov et al. [5], Chernyi [6], Zheltovodov [7], Knight et al. [8] and Fomin et al. [9].

Levin et al. [10] numerically studied the effects of energy deposition on aerodynamic drag and heat transfer of blunt body and predicted the limitation of drag reduction. Zheltovodov et al. [11] carried out a 2D unsteady numerical simulation for a Mach 3.45 flow. The results were compared with Adelgren et al. [12, 13] and Tretyakov et al. [14, 15] experiments. Riggins et al. [16, 17] numerically compared different wave drag reduction techniques. The results showed that the method of energy deposition had the greatest drag reduction capability and highest efficiency. Adelgren et al. [18] carried out a series of experiments to study the influence of energy deposition on hemisphere in Mach 3.45 flow. The stagnation pressure showed a 40% reduction. Erdem et al. [19, 20] carried out experiments in Mach 5 flow with arc discharge and analyzed the effect of different configuration. Sakai et al. [21], Sasoh et al. [22, 23] and Kim et al. [24, 25] carried out a series of numerical and experimental studied of energy deposition in Mach 2 flow and a 21% drag reduction was achieved in the experiments. Tate et al. [26] developed a non-equilibrium thermal chemical code to simulate the air ionization, and the interaction of blast wave and bow shock. Kremeyer [27] and Kremeyer et al. [28] studied the effects of pulsed energy lines on drag reduction. It showed advantages over pointed energy deposition.

The objective of the present study was to further understand the mechanism of wave drag reduction by energy deposition in Mach 8 flow and to explore the key factors in improving the efficiency of drag reduction. A numerical simulation was performed for the parametric study, which was difficult to realize by experiments. Although the energy deposition process is a multi-disciplinary process including electron release, gas ionization, plasma formation, and blast wave propagation, the previous studies [8,

12, 31] have shown that the main mechanism of wave drag reduction is the blast wave interaction. Therefore, this paper focused on the aerodynamic effects of the laser energy deposition in the flow field.

2. FLOW CONFIGURATION AND NUMERICAL METHOD

A two dimensional flow was modeled based on the experiments [29, 30], in which a Mach 8.04 flow was past a cylinder with diameter of 76 mm. The flow domain is sketched in Fig.1, where the origin of the coordinates lies on the stagnation point of the cylinder.

The static pressure and temperature at freestream were 855 Pa and 123.5 K, respectively. In the case of energy deposition, the laser energy was modeled as a sphere with uniformly distributed temperature and pressure, and was positioned in front of the cylinder on the x axis. The process of ionization was not considered in the present study.

The energy input by laser spot can be expressed by the following equation:

$$E = \rho_{\infty} c_v \Delta T V \quad (1)$$

where ρ_{∞} is the freestream density, c_v is the specific heat at constant volume, ΔT is the temperature increase due to energy deposition, and V is the laser focal volume, which was assumed as a sphere [31]. A dimensionless parameter ε was defined to evaluate the relative input energy to the flow:

$$\varepsilon = \frac{E}{E_l} \quad (2)$$

where E_l is the enthalpy of the local flow field without energy deposition, and can be expressed as:

$$E_l = \rho_{\infty} c_p T_{\infty} V \quad (3)$$

The two dimensional inviscid simulations were carried out with the commercial flow solver FLUENT. The second order accurate AUSM scheme was adopted for convective flux term and the first order implicit method was used for temporal discretization. The gradient reconstruction was based on node Green-Gauss method. Equations were solved using incomplete lower upper factorization (ILU), in conjunction with algebraic multigrid (AMG) method. The pressure far field condition was used for the inflow and outflow, where the Mach number, static pressure and temperature were fixed.

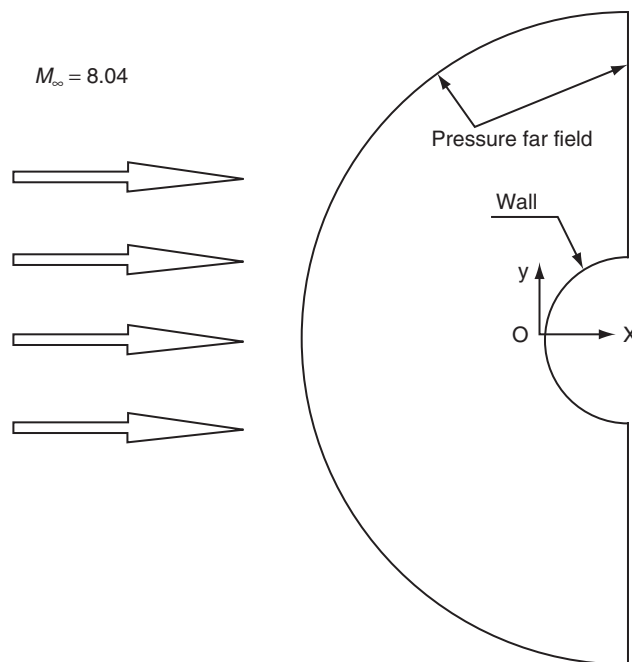


Figure 1. Flow configuration.

3. RESULTS AND DISCUSSION

3.1. Baseline Flow

The flow without energy deposition was simulated first. The grids were uniformly distributed at one cylinder radius away from the surface, and then stretched along the radial direction with a ratio of 1.02. A grid refinement study was performed through six grid configurations. The grid information is listed in Table 1, where Δ_{th} is the standoff distance predicted by the empirical formula proposed by Ambrosio and Wortman [32] for 2D bow shock:

$$\Delta_{th} = 0.386R \cdot \exp\left(\frac{4.67}{M_\infty^2}\right) \quad (4)$$

where R is the radius of the cylinder. For the case with $M_\infty = 8.04$, $R = 38$ mm, we can get $\Delta_{th} = 15.8$ mm.

Fig. 2 showed the pressure distribution along the cylinder surface normalized by $p_{0,th}$, which was the theoretical pressure at the stagnation point. It was shown that all the grid configurations predicted the surface pressure well. To identify the accuracy, the error of stagnation pressure was defined as:

$$\varepsilon_p = 1 - \frac{p_{0,base}}{p_{0,th}} \quad (5)$$

where $p_{0,base}$ is the computed pressure at the stagnation point for the baseline case. It was shown in Fig. 3 that ε_p first decreased with the increase of the number of grid layers in the standoff distance, then showed a small variation, and finally leveled off. Grid No. 3 had a similar ε_p value, but a less grid number, compared with Grid No. 6, therefore was adopted for the simulations.

The computed surface pressure was compared with experiments [30] as shown in Fig. 4. The computational results were in good agreement with the experimental data. The computed standoff

Table 1. Grid refinement

| Grid no. | Grid number | Number of grid layers in Δ_{th} |
|----------|--------------------|--|
| 1 | 6×10^4 | 50 |
| 2 | 1.35×10^5 | 75 |
| 3 | 2.40×10^5 | 100 |
| 4 | 3.75×10^5 | 125 |
| 5 | 5.4×10^5 | 150 |
| 6 | 1.22×10^6 | 225 |

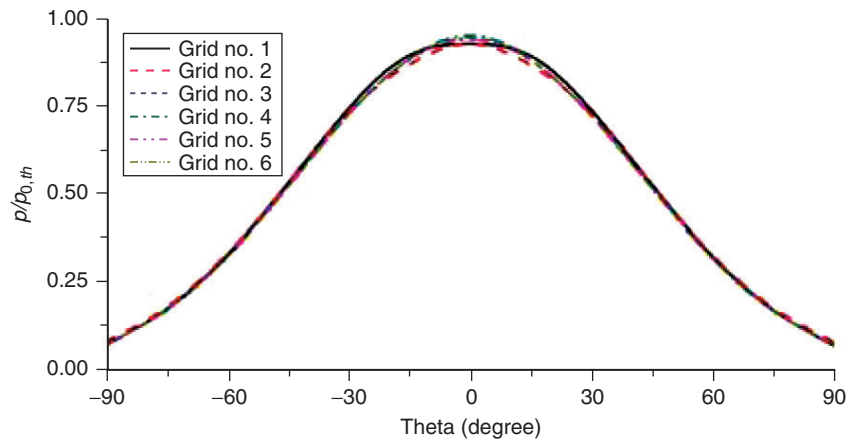


Figure 2. Surface pressure distribution at different grid numbers.

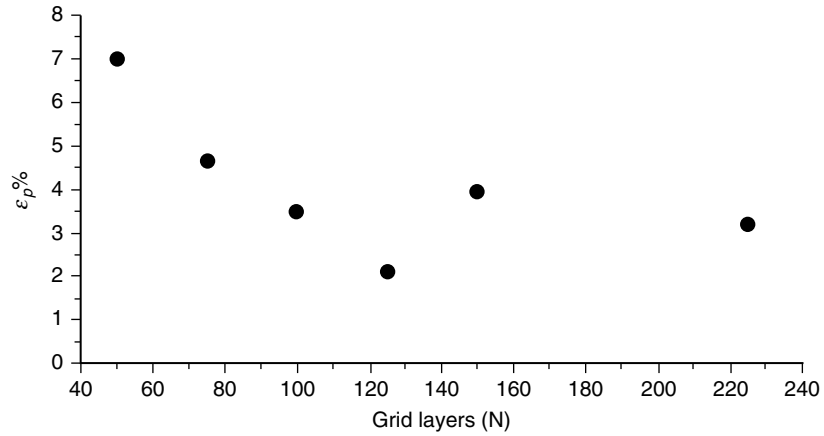


Figure 3. Error of stagnation pressure at different grid numbers.

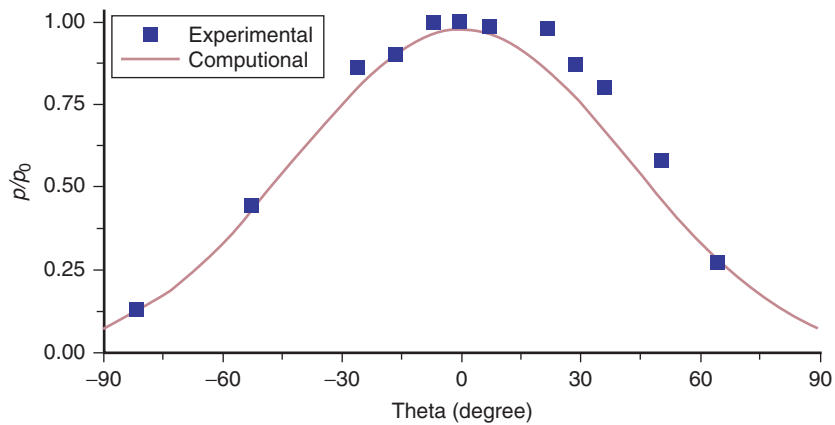


Figure 4. Surface pressure compared with experimental data.

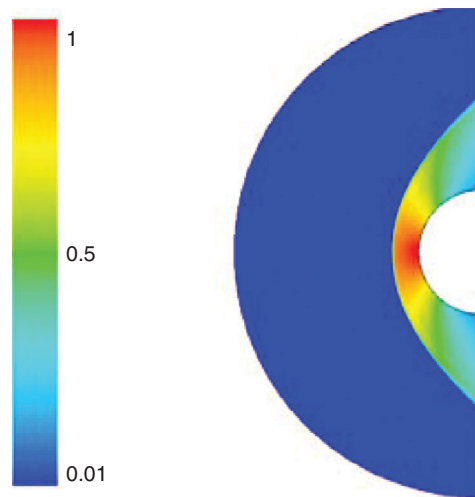


Figure 5. Pressure contours.

distance is 16.5 mm, and its error was about 4% compared with the theoretical value. Figs. 5 and 6 showed the contours of pressure and temperature, respectively. The pressure and temperature was greatly increased after the bow shock, which intensified the aerodynamic force and heating in the front surface of the cylinder.

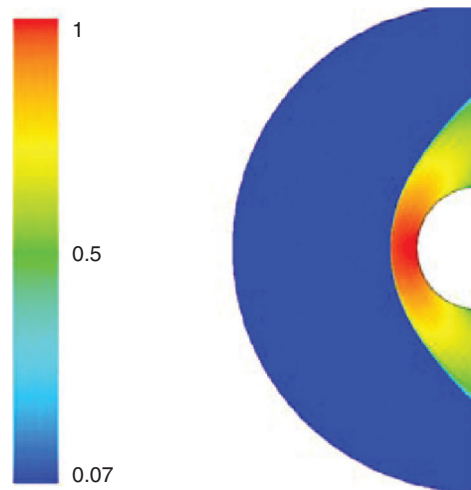


Figure 6. Temperature contours.

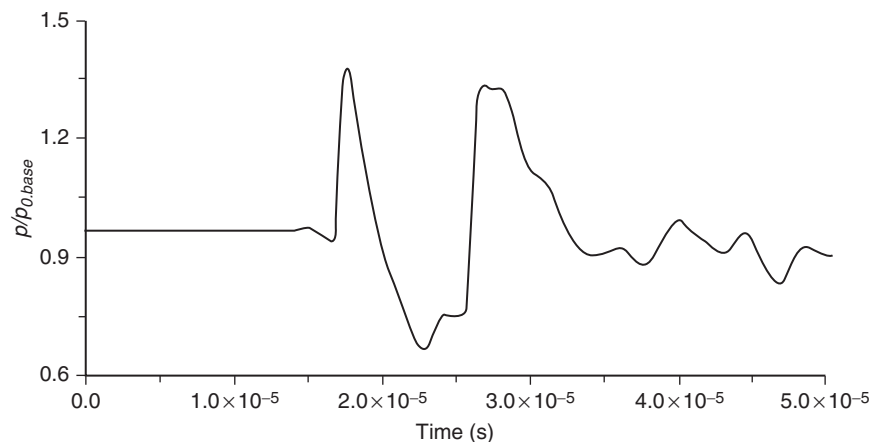
3.2. Laser Energy Deposition

3.2.1. Flow Field of Energy Deposition

Once the baseline was obtained, an energy spot was deposited upstream of the bow shock. As a reference case, we considered the condition of energy level $\varepsilon = 100$ with a single laser pulse. The center of the focal zone was located on the x axis and $2/3R$ away from the cylinder. The time step was taken as 1×10^{-9} s.

The time history of the pressure at the stagnation point was plotted in Fig. 7. The surface pressure experienced the first peak at about 1.8×10^{-5} s when the front of the blast wave stroke the surface. Then the pressure began to decrease as the expanded low pressure region behind the blast wave front reached the surface. The second peak pressure was formed when the trailing edge of the blast wave stroke the surface. During the last stage, a series of weak waves reflected and interacted near the surface, resulting in the surface pressure fluctuation.

Four numerical schlieren images were shown in Fig. 8 to demonstrate the interaction of the energy spot with the bow shock and surface. Once the energy was deposited, a blast wave was formed and propagated outward from the spot center. Meanwhile it expanded and moved downstream towards the surface. At about 4.4×10^{-6} s (Fig. 8 (a)), the leading edge of the blast wave interacted with the bow shock. The blast wave was compressed and concaved inside. The transmitted wave moved on and stroke the cylinder surface which resulted in the pressure increase at $t = 1.8 \times 10^{-5}$ s (Fig. 8 (b)). Then the expansion waves were transmitted to the surface, which reduced the pressure (Fig. 8 (c)). A pair of vortices was formed along the slipstreams downstream to the intersections of the blast wave and the

Figure 7. Time history of surface pressure at stagnation point for $\varepsilon = 100$.

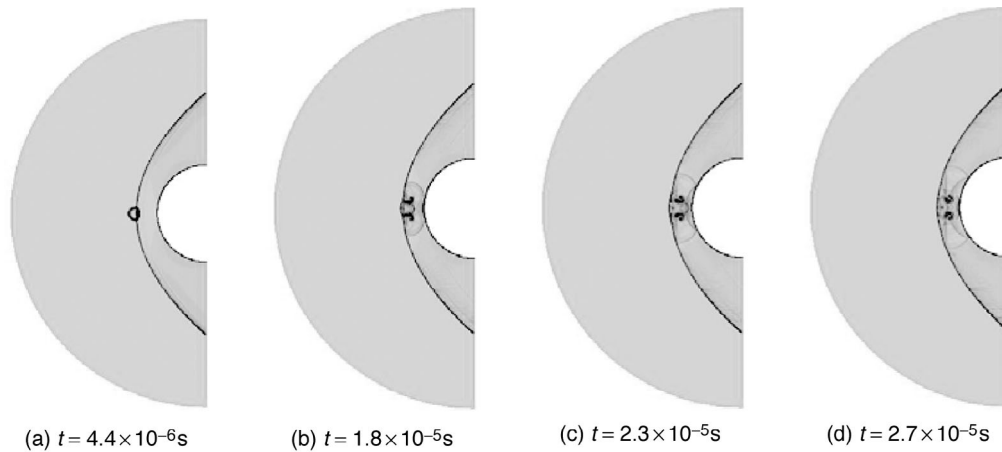


Figure 8. Numerical schlieren images at different times.

bow shock. In the later stage of the flow development, the trailing edge of the blast wave stroke the surface, and was accompanied by a series of wave reflection and interaction (Fig. 8 (d)).

The time-averaged pressure p_{avg} normalized by $p_{0,base}$ along the surface was shown in Fig. 9. The time-averaged values were based on the time duration which was measured from the time instant of energy deposition to the moment of flow field returning to its undisturbed state. The baseline case was plotted for reference. Due to energy deposition, the surface pressure was reduced and the stagnation pressure was reduced by 3%, showing the possibility of wave drag reduction.

3.2.2. Effect of Energy Level

Four different energy levels ($\epsilon = 1, 50, 100$ and 200) were computed, respectively. The energy deposition location was the same with the reference case in section 3.2.1. Fig. 10 showed the time history of the stagnation pressure at different energy levels. Although the peak pressure increased with the energy level, the minimum pressure also decreased with an extended duration.

Fig. 11 showed the time-averaged surface pressure at different ϵ . It was observed that, when $\epsilon = 200$, the pressure reduction in the stagnation region was relatively large; while when $\epsilon < 200$, the pressure reduction kept almost the same. It was shown that, for a given deposition location, the energy level should be increased to a certain level to have significant influence. Besides, the reduction level at $\epsilon = 50$ was shown to be a little bit larger than that at $\epsilon = 100$. This might be caused by the nonlinearity between the energy level and the pressure reduction

3.2.3. Effect of Deposition Location

Four deposition locations were considered, namely $2/3R$, R , $4/3R$ and $1.9R$ away from the cylinder on the x axis. The energy level was $\epsilon = 100$. Fig. 12 showed the time history of the stagnation pressure. It

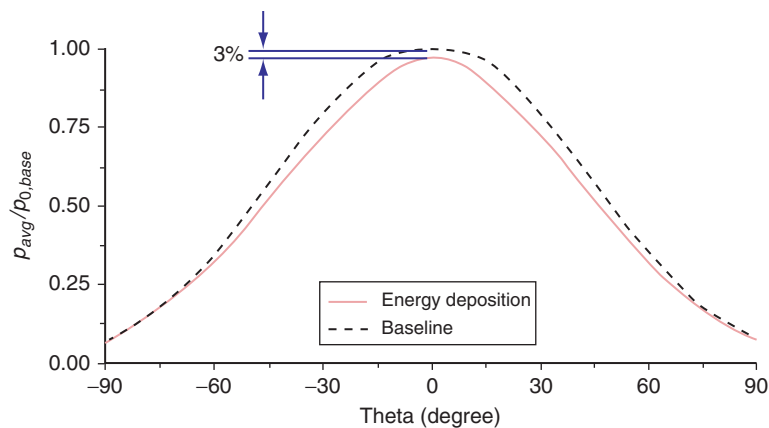


Figure 9. Time-averaged surface pressure distribution.

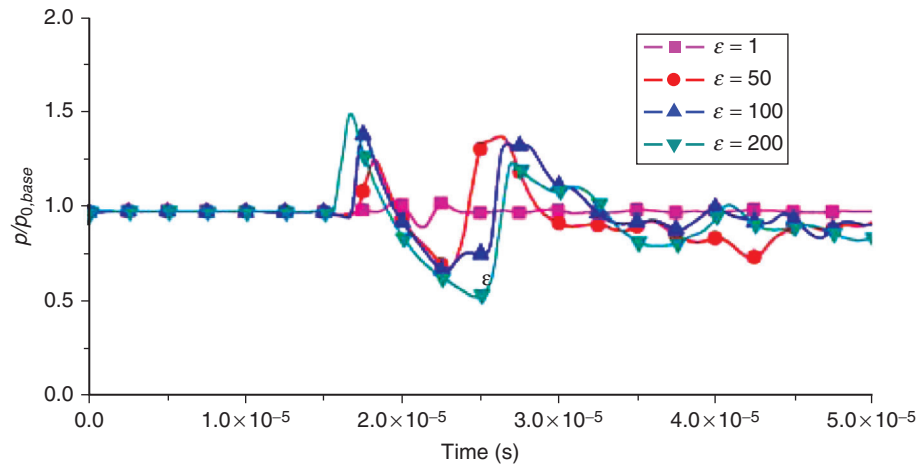


Figure 10. Time history of stagnation pressure at different ε .

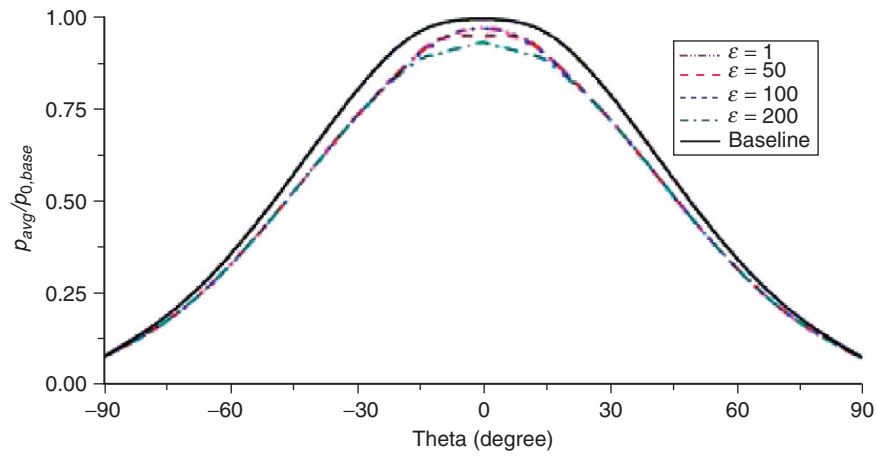


Figure 11. Time-averaged surface pressure at different ε .

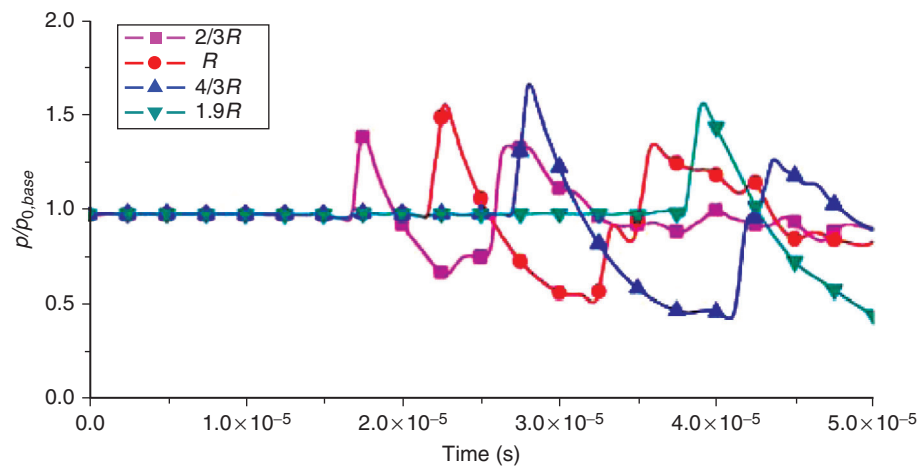


Figure 12. Time history of stagnation pressure at different locations.

is shown that, with the increase of distance, the time duration that the stagnation point experienced the first peak pressure was enlarged. And the peak value first increased with the distance and then decreased. Fig. 13 showed the surface pressure at different deposition locations. The reduction of the

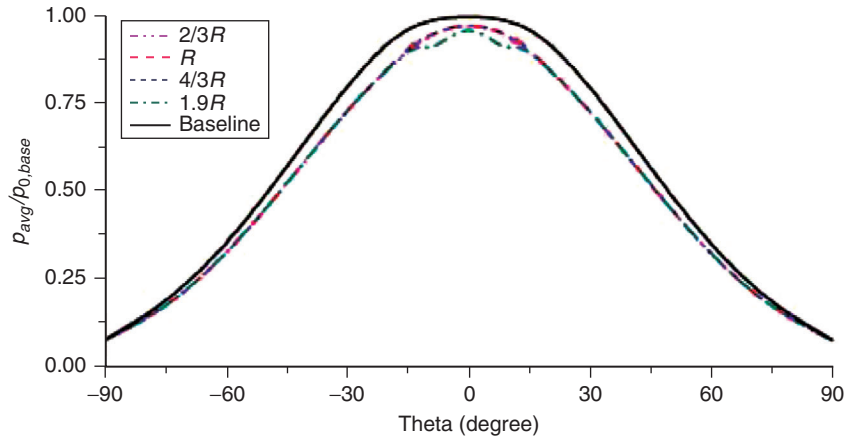


Figure 13. Time-averaged surface pressure at different locations.

pressure kept almost the same when the distance was less than $4/3R$. As the distance further increased, the time-averaged surface pressure reduced relatively large.

3.2.4. Effects of Pulsing Frequency

Four pulsing frequencies ($f = 10, 25, 50$ and 100 kHz) with energy level $\varepsilon = 100$ were studied. Fig. 14 showed the surface pressure distribution at different frequencies. The result showed that the frequency was an important factor that had great effect on the surface pressure variation. With the increase of frequency, the time-averaged surface pressure was greatly reduced. When the frequency reached 100 kHz, the time-averaged stagnation pressure reduced 33% of the baseline. There were three peak pressure positions along the surface. This may relate to the pair of the vortices near the stagnation region.

Fig. 15 showed the numerical schlieren images for four frequencies when the flow field reached an asymptotic state. When the frequency was low, the effect of blast wave on the bow shock between pulses was isolated as shown in Fig. 15 (a). With the increase of frequency, the blast wave began to have superposition effects on the bow shock (Fig. 15 (b)). When the frequency reached 50 kHz, the interaction of the blast wave and bow shock was evident (Fig. 15 (c)). And when the frequency reached 100 kHz, the envelope of the blast wave formed a conical shock wave (Fig. 15 (d)). A continual low pressure region was formed in front of the blunt body; therefore the wave drag was reduced.

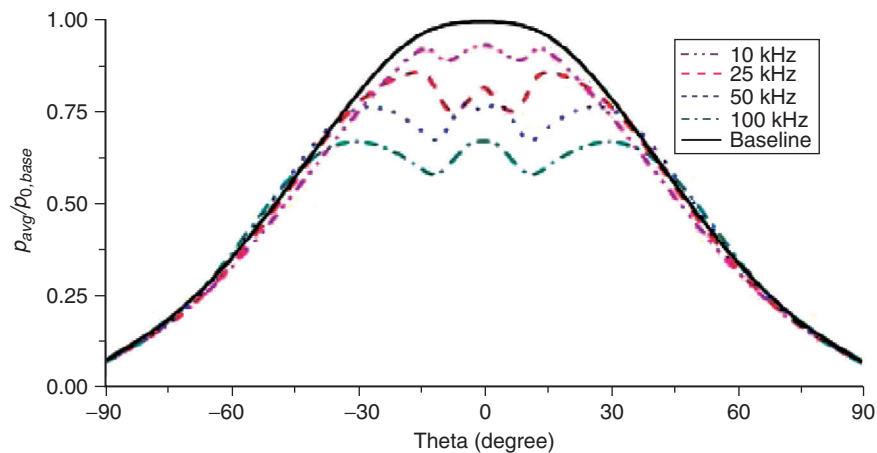


Figure 14. Time-averaged surface pressure at different frequencies.

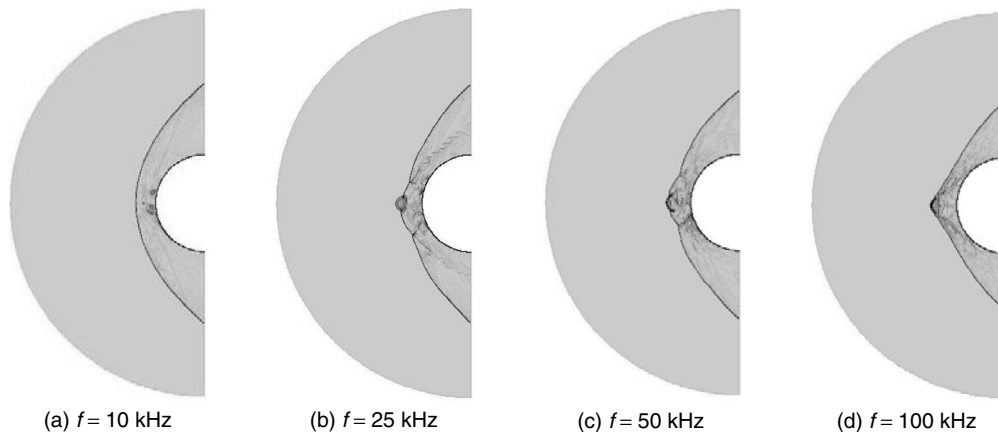


Figure 15. Numerical Schlieren images at different frequencies.

4. CONCLUSION

A parametric study of laser energy deposition in a Mach 8 bow shock was performed to further understand the feasibility of this technique. The computational results were in good agreement with the theoretical standoff distance and experimental surface pressure. The flow field with energy deposition in the Mach 8 flow was analyzed. The interaction process of blast wave and bow shock was revealed. The effect of energy level, deposition location and pulsing frequency was analyzed. Results showed that frequency was the key parameter to the wave drag reduction. A 33% reduction of stagnation pressure was realized at a frequency of 100 kHz.

ACKNOWLEDGEMENTS

This work is supported by National Natural Science Foundation of China.

REFERENCES

- [1] B. Spencer Jr., Hypersonic aerodynamic characteristics of minimum-wave-drag bodies having variations in cross-sectional shape, *NASA TN D-4079*, 1967.
- [2] D. Bivolaru, and S.P.Kuo, Observation of supersonic shock wave mitigation by a plasma aerospike, *Physics of Plasmas*, Vol.9, No. 2, 2002: 721–723.
- [3] D. M. Bushnell, Shock wave drag reduction, *Annul. Rev. Fluid Mech.*, 2004.38: 81–96.
- [4] K. Oswatitsch, Propulsion with heating at supersonic speed, *Deutsche Versuchsanstalt fur Luft und Raumfahrt, Rept.90, Berlin*, 1959.
- [5] P. K. Tretyakov, V.Fomin, and V. I. Yakovlev, New principle of control of aerophysical process, *Proc. International Conference on the Methods of Aerophysical Research*, 1996: 210–220.
- [6] G. G. Chernyi, The impact of electromagnetic energy addition to air near the flying body on its aerodynamics characteristics, *Proceedings of the 2nd Weekly Ionized Gases Workshop*, 1998:1–31.
- [7] A. A. Zheltovodov, Development of the studies on energy deposition for application to the problems of supersonic aerodynamics, *Preprint No. 10-2002, Institute of Theoretical and Applied Mechanics, Russian Academy of Sciences, Siberian Branch, Novosibirsk*, 2002.
- [8] D. D. Knight, V. Kuchinskiy, A. Kuranov, and E. Sheikin, Survey of aerodynamic flow control at high speed by energy deposition, *AIAA Paper*, 2003–0525.
- [9] V. Fomin, P. Tretyakov, and J. P. Taran, Flow control using various plasma and aerodynamic approaches (shot review), *Aerosp. Sci. and Tech.*, No. 8, 2004: 411–421.
- [10] V. A. Levin, V. G. Gromov, and N. E. Afonina, Numerical analysis of the effect of local energy supply on the aerodynamic drag and heat transfer of a spherically blunted body in a supersonic air flow, *J. App. Mech. Tech. Phys.*, Vol. 41, No. 5, 2000: 915–922.
- [11] A. A. Zheltovodov, E. A. Pimonov, and D. D. Knight, Energy deposition influence on supersonic flow over axisymmetric bodies, *AIAA Paper*, 2007–1230.

- [12] R. G. Adelgren, G. Elliott, D. D. Knight, A. A. Zheltovodov, and T. Beutner, Energy deposition in supersonic flow, *AIAA Paper*, 2001–0885.
- [13] R. G. Adelgren, H. Yan, G. Elliott, D. D. Knight, T. Beutner, A. A. Zheltovodov, and M. Ivanov, Localized flow control by laser energy deposition applied to Edney IV shock impingement and intersection shocks, *AIAA Paper*, 2003–0031.
- [14] P. K. Tretyakov, A. F. Garanin, G. P. Grachev, V. L. Kraynev, A. G. Ponomarenko, V. N. Tishenko, and V. L. Yakovlev, The supersonic flow control over the bodies with the use of power optical pulsating discharge, *Dokladi Akademii Nauk (DNA)*, Vol. 351, No. 3, 1996: 339–340.
- [15] P. K. Tretyakov, A. F. Garanin, and V.I. Yakovlev, Investigation of local laser energy release influence on supersonic flow by methods of aerophysical experiments, *Proc: International Conference on the Methods of Aerophysical Research*, 1996: 200–204.
- [16] D. W. Riggins, H. F. Nelson, and E. Johnson, Blunt body wave drag reduction using focused energy deposition, *AIAA Paper*, 98–27875.
- [17] D. W. Riggins, J. T. Barnett, and T. T. Taylor, Drag Reduction and Heat Transfer Mitigation Techniques for Blunt Bodies in Hypersonic Flight, *AIAA Paper*, 2003–6968.
- [18] R. G. Adelgren, H. Yan, G. S. Elliott and D. D. Knight, Drag and total power reduction for artificial heat input in front of hypersonic blunt bodies, *AIAA J.*, Vol. 43, No. 2, 2005: 256–269.
- [19] E. Erdem, L. Yang, and K. Kontis, Drag Reduction by Energy Deposition in Hypersonic Flows, *AIAA Paper*, 2009–7374.
- [20] E. Erdem, L. Yang, and K. Kontis, Drag Reduction Studies by Steady Energy Deposition at Mach 5, *AIAA Paper*, 2011–1027.
- [21] T. Sakai, Y. Sekiya, M. Rosli, A. Matsuda, and A. Sasoh, Unsteady interaction of blunt bodies with laser induced plasma in a supersonic Flow, *AIAA Paper*, 2008–3794.
- [22] A. Sasoh, Y. Sekiya, T. Sakai, J. H. Kim and A. Matsuda, Drag reduction of blunt body in a supersonic flow with laser energy depositions, *AIAA Paper*, 2009–1533.
- [23] A. Sasoh, Y. Sekiya, T. Sakai, J. H. Kim, and A. Matsuda, Supersonic drag reduction with repetitive laser pulses through a blunt body, *AIAA J.*, Vlo. 48, No. 12, 2010: 2811–2817.
- [24] J. H. Kim, A. Matsuda, T. Sakai, and A. Sasoh, Drag reduction with high-frequency repetitive side-on laser pulse energy depositions, *AIAA Paper*, 2010–5104.
- [25] J. H. Kim, A. Matsuda, T. Sakai and A. Sasoh, Wave drag reduction with acting spike induced by laser-pulse energy depositions, *AIAA J.*, Vol. 49, No. 9, 2011: 2076–2078.
- [26] M. Tate, Y. Ogino, and N. Ohnishi, Thermochemical nonequilibrium flow computation of drag reduction by pulsed laser, *AIAA Paper*, 2010–1535.
- [27] K. Kremeyer, Lines of pulsed energy for supersonic/hypersonic drag reduction, *AIAA Paper*, 2004–984.
- [28] K. Kremeyer, K. Sebastian, and C. W. Shu, Computational Study of Shock Mitigation and Drag Reduction by Pulsed Energy Lines, *AIAA J.*, Vol. 44, No. 8, 2006: 1720–1731.
- [29] M. S. Holden, and J. R. Moselle, A database of aerothermal measurements in hypersonic flow for CFD validation, *AIAA Paper*, 92–4023.
- [30] A.R. Wieting, and M. S. Holden, Experimental shock-wave interference heating on a cylinder at Mach 6 and 8, *AIAA J.*, Vlo. 27, No. 11, 1989: 1557–1565.
- [31] H. Yan, R. G. Adelgren, M. Boguszko, and D. D. Knight, Laser energy deposition in quiescent air, *AIAA J.*, Vlo. 41, No. 10, 2003: 1988–1995.
- [32] A. Ambrosio, and A. Wortman, Stagnation point shock detachment distance for flow around spheres and cylinders, *ARS J.*, 32, 1962.